Integral Equation Study of the Solvation Force between Macroscopic Surfaces Separated by Thin Films of Diatomic, Chain, and Network Solvents

Yurko Duda,[†,‡] Douglas Henderson,[§] Andrij Trokhymchuk,*[,†,‡] and Darsh Wasan[||]

Instituto de Química, UNAM, Coyoacán, 04510, México D.F., and Brigham Young University, Provo, Utah 84602, and Illinois Institute of Technology, Chicago, Illinois 60616

Received: April 12, 1999; In Final Form: June 25, 1999

The simple models of associating fluids, i.e., hard spheres with one, two, and four surface-located associatively interacting sites are employed in the singlet approach of integral equation theory to probe the effects of the nonsphericality of solvent molecules: linear and branched (or network) chain formations in the solvent on the interaction between two immersed macroscopic surfaces. We found that the obtained results qualitatively reproduce the most important experimentally observed features of the solvation force. We see what may be called negative solvation forces between macroscopic surfaces in a linear chain solvent, whereas in the case of the network solvent, the solvation force is nearly monotonic, positive, and repulsive at short separations.

I. Introduction

Many experimental and theoretical studies are aimed at understanding the phenomenon of the stabilization of liquid surfactant films and, thereby, the stabilization of dispersions, such as emulsions, foams, etc. The ability of a dispersion to flocculate is ultimately determined by the force acting between the surfaces of colloidal particles as they approach in a solvent. This force can be separated into two contributions, i.e., one arises from the direct interaction between surfaces and the other is exerted by the interfacial solvent film. At present, the first contribution is well understood: if the colloidal particles are uncharged, this is the attractive van der Waals forces (also known as dispersion or Hamaker forces) between two macrosurfaces, considered in the classical DLVO theory. The second contribution is usually referred to as the solvation or structural or depletion force. It results from the difference between the normal stress acting on the inner side of the surfaces separated by the solvent film, and pressure exerted by the bulk fluid on the outer side. When the solvent particles are uncharged and the film thickness is sufficiently large (of the order of 10 times of solvent particle diameters, or of 10 times of the largest solvent particle diameters in the case when the solvent is a dispersion) the pressures in the bulk and in the film are the same, and the van der Waals forces dominate, causing surfaces to approach. These hypotheses agree well with experimental observations. But once the film has thinned to less then a few solvent particle diameters, the normal component of pressure in close confinement of solvent molecule becomes oscillatory, resulting in an oscillatory behavior of the total force between the confinement surfaces. It follows that the predictions of the continuum DLVO theory break down for the treatment of the short-range interaction between colloidal particles. The discrete molecular nature of the solvent becomes essential for the correct description of the thin film contribution to the force acting between confining surfaces. An attempt to add a hard-core exclusion contribution (the effect of the finite size of solvent molecule) to the DLVO theory has been done by Henderson and Lozada-Cassou[1] and Henderson.[2] It has been shown that it is the origin of the oscillations in the total force due to the almost perfect layering of hard-sphere solvent molecules. The same conclusion follows from the computer simulation studies for spherical solvent molecules.[3−6] Further effects result[7] from the shape of the solvent molecules, the composition and polydispersity of the solvent, the interaction between solvent molecules, the interaction of solvent molecules with substrate surfaces, and the structure of the surfaces.

Although of large practical importance and in spite of intense research endeavors on confined molecular solvents of different molecule shapes, which include octane and *n*-alkanes, they are poorly understood.[8−10] The development of Israelachvili's "surface force apparatus" has permitted the direct experimental probing of the intersurface forces and clearly shows the peculiarity of such solvents. Particularly, from the experimental observations it appears that a mixture of differently shaped molecules[11] cannot order themselves into coherent layers so that the range of the short-range structure becomes even shorter and, for nonlinear and branched chain molecules,[12] the liquid film remains disordered or amorphous and the measured force is not oscillatory but monotonic. Such tendencies have been obtained recently from computer simulations of linear and branched solvent molecules.[13−17] In the main part, such peculiarities are caused by the structure of the thin liquid films. But the simultaneous experimental measurement of the force and the confined liquid structure is difficult and indirect due to the small amount of material present. This gap can be fulfilled by theory. One of the best opportunities to meet such need result from computer experiment methods. The virtue of these methods is that they are applicable to realistic molecular models. Computer experiments on atomistic model fluids performed not so far[13−17] have provided considerable insight, but are expensive and limited in regard to accessible time scales, molecular size, and ability to compute the small solvation forces characteristic of the confinement at distances of common experimental interest. Another possibility is to apply the methods of integral equation

[†] Instituto de Química.

[‡] Permanent address: Institute for Condensed Matter Physics, National Academy of Sciences of the Ukraine, 290011 Lviv, Ukraine. E-mail: adt@icmp.lviv.ua.

[§] Brigham Young University.

[||] Illinois Institute of Technology.

10.1021/jp991193j CCC: $18.00
Published on Web 08/18/1999

theory[18−23] or density functional theory,[24,25] though they are limited by modeling possibilities. This limitation seems not to be great importance when one aims to obtain an insight into the nature of phenomenon.

In this paper we aim to mimick solvents with differently shaped molecules by using the ideas and models from the integral equation theory of homogeneous associating fluids. Namely, we consider the hard spheres with one, two, and four attractive sites. One- and two-site homogeneous models, which describe dimerizing and polymerizing fluids, respectively, have been investigated intensively.[26,27] The four-site model can describe symmetrical and non-symmetrical networks which may consist of very complicated aggregates (e.g., linear branches, loops, crossing rings, etc.) which require more and more refined description. Therefore, this model is able to reproduce various kinds of macromolecules and a network of bonds by appropriate choices of the energy parameter. The latter can be regarded as mimicking the topology of hydrogen bonding in water, in ammonia or in methanol. Some of such possibilities have been studied in refs 28 and 29, where an associative integral equation approach to this model has been developed.

The rapid development of the theory of homogeneous associating fluids during the last decade[27−35] has stimulated investigations of the behavior of such systems under the influence of external potential fields, for example, in contact with solid surfaces.[36−41] On the basis of the associative version of Henderson−Abraham−Barker (HAB) integral equation,[42] the properties of one-, two- and four-site models near the hard wall have been studied.[36−38]

The slit-like pore is the next step in the complication of the confinement. The equilibrium partitioning of a hard-sphere solvent in a slitlike pore has been studied by using integral equation techniques.[43] More complicated geometrical confinement, such as spherical or cylindrical pores, or other geometries, as well as different solvent models of spherically shaped molecules have also been extensively studied.[24,43−47] Recently, the properties of dimerizing fluids in slit-like pores has been addressed by Trokhymchuk et al.[22,23] The density profiles of fluid particles inside the pore, the adsorption isotherms, and the solvation force acting between the walls of the pore have been investigated.

In the present work, we attempt to apply the HAB approach to investigate the changes in the film properties, as affected by the different shape and architecture of the solvent molecules. The main attention is paid to the local density distributions in the films formed by dimer, linear and branched chains and its relation with the trends of the changes in the force acting between confining surfaces.

II. Modeling

Let us imagine that we have a huge reservoir of volume V filled by the fluid solvent with a number particle density $\bar{\rho} = N/V$, which we will call "bulk". In one part of this reservoir we immersed two planar surfaces that are infinite in area separated by distance H. The fluid in between the surfaces will form the fluid film and is in equilibria with the bulk fluid.

Four different types of solvents that consist of spherical monomers (MON), dimers (DIM), linear chains or polymers (POL), and branched or network chains (NET) will be considered. To model such solvents, we use a system of hard-sphere particles, hard spheres with each sphere containing one, two, and four embedded attractive sites, respectively. For each model the hard-core diameter d, is assumed to be the same, we will use, therefore d as the length unit, i.e., $d = 1$. It follows that parameter $\rho = \bar{\rho}d^3$ will correspond to the reduced number density, and parameter $\eta = \pi\rho/6$ will define the volume fraction of each solvent. For models with two and four sites, the sites located on the same particle are assumed to be independent on each other. This means that the bonded state of a given site does not affect the bonding at the other sites of the same fluid particle. This contrasts with the primitive model of water discussed by others,[33,34] where the sites were arranged with tetrahedral symmetry. This assumption allows us to avoid considering angular restriction effects.

In general, the pair interaction $U(\mathbf{1}, \mathbf{2})$ between two particles **1** and **2** for these models consists of the hard-sphere repulsive term $U^{HS}(r)$ and a contribution describing site−site interaction, i.e.,

$$U(\mathbf{1}, \mathbf{2}) = U^{HS}(r) + \sum_a \sum_b U_{ab}^{AS}(\mathbf{1}, \mathbf{2}) \tag{1}$$

where **1** and **2** denote the position and orientations of the two particles; a and b are the sites on the particle **1** and **2**, respectively. As usual, the hard-sphere repulsion is written in the form

$$U^{HS}(r) = \begin{cases} \infty, & r < 1 \\ 0, & r \geq 1 \end{cases} \tag{2}$$

The term $U_{ab}^{AS}(\mathbf{1}, \mathbf{2})$ denotes the potential for a short-ranged and highly directional attractive interaction between site a on particle **1** and site b on particle **2** and is given in the square-well form

$$U_{ab}^{AS}(\mathbf{1}, \mathbf{2}) = \begin{cases} -\epsilon_{ab}, & x_{ab} < x_c \\ 0, & x_{ab} \geq x_c \end{cases} \tag{3}$$

Here x_{ab} is the distance between the sites a and b of the molecules **1** and **2**, respectively; ϵ_{ab} is the depth of the potential well, and x_e is the range of associative interaction. We note that $U_{ab}^{AS}(\mathbf{1}, \mathbf{2}) = 0$ for monomer fluid, $\{a,b\} = \{1\}$ for dimer fluid, $\{a,b\} = \{1,2\}$ for linear chain fluid, $\{a,b\} = \{1,2,3,4\}$ in the case of network forming fluid.

The one- and two-site models can describe dimerizing and polymerizing flexible linear chain solvents, respectively. The hard-sphere model with four attractive sites is a much more complicated model, which is able to describe the formation of various associating aggregates such as branched polymer chains and a network of bonds. These four types of models are a suitable set of nonpolar molecular solvents covering the range of different sizes, rigidity, and shapes, and the models allow us to provide a qualitative comparison with experimentally studied liquids.[48]

To describe the interaction of the fluid species with a confinement, we assume that the surfaces of the immersed substrates are structureless surfaces located at $z = 0$ and $z = H$ can attract or repel adsorbed fluid particles. To model such systems we used the following potential

$$U_S(z,H) = \begin{cases} \infty, & z \leq 0 \text{ or } z \geq H \\ \phi(z) + \phi(H - z), & 0 < z < H \end{cases} \tag{4}$$

where z is the distance between the center of fluid particle and the surface in the direction perpendicular to the surface. Such a form for the potential $U_S(z, H)$ implies that the fluid particle center can be located on the surface either at $z = 0$ or $z = H$ and actual film thickness is $H + d$. The function $\phi(z)$ is modeled by the Lennard-Jones (9,3) potential,

$$\phi(z) = \epsilon_S\left[\left(\frac{z_S}{z}\right)^9 - \alpha\left(\frac{z_S}{z}\right)^3\right] \quad (5)$$

where parameters ϵ_S and z_S have the same meaning as for usual (12,6) Lennard-Jones potential, and switching parameter $\alpha = 0$ for repulsive (lyophobic) surfaces and $\alpha = 1$ for attractive (lyophilic) surfaces.

III. Integral Equation Theory Background

Application of the integral equation method to the inhomogeneous system described above is based on the HAB integral equation, derived originally by Henderson, Abraham, and Barker[42] for the hard-sphere fluid. In the case of a monomer fluid it can be rewritten as follows

$$y^{MON}(z_1, H) = 1 + 2\pi\int_{|z_1-1|}^{z_1+1}\rho S^{MON}(|z_{12}|)h^{MON}(z_2, H)dz_2 \quad (6)$$

with

$$S^{MON}(|z|) = \int_{|z|}^{1} tC(t)^{MON}dt \quad (7)$$

where $z_{12} = z_1 - z_2$, ρ is the bulk fluid density, $h^{MON}(z, H)$ and $y^{MON}(z, H)$ are the fluid−surface pair and cavity correlation functions, respectively, related by definition

$$h^{MON}(z, H) = \gamma(z, H)y^{MON}(z,H) - 1 \quad (8)$$

and $\gamma(z, H)$ is the Boltzmann factor for the fluid−surface interaction 4. The key element of the whole scheme is the function $S^{MON}(r)$ in eq 6 which is defined through the function $C^{MON}(t)$ being the bulk fluid direct correlation function at density ρ. It is the only bulk information needed to solve the HAB equations. In general it can be extracted from any source, including computer experiment. In the present study we will do this from the solution of the bulk fluid Ornstein−Zernike equation in the Percus−Yevick (PY) approximation by the Baxter factorization method. The convenience of this method in our particular case comes from the fact that the *S*-function defined by eq 7 can be obtained implicitly in analytical form, and in such way we avoid the additional integration step in the solution of eq 6. The PY solution for a bulk hard-sphere fluid has been obtained in original work of Baxter,[49] and function $S^{MON}(r)$ has the form

$$S^{MON}(r) = \frac{1}{2}a_0(r^2 - 1) + b_0(r - 1) - 2\pi\rho\left(\frac{1}{4}A_1a_0^2 + \frac{1}{2}(A_2 + A_3)a_0b_0 + A_4b_0^2\right) \quad (9)$$

where

$$a_0 = \frac{1 + 2\eta}{(1 - \eta)^2}, \quad b_0 = -\frac{3\eta}{2(1 - \eta)^2} \quad (10)$$

and

$$A_1 = \frac{8}{15} - \frac{1}{2}r - \frac{2}{3}(r^2 - r^3) - \frac{1}{30}r^5,$$
$$A_2 = \frac{5}{12} + \frac{1}{12}r^4 + \frac{1}{3}r^3 - \frac{1}{2}r^2 - \frac{1}{3}r,$$
$$A_3 = \frac{5}{12} - \frac{2}{3}r + \frac{1}{3}r^3 - \frac{1}{12}r^4, \quad A_4 = \frac{1}{3} - \frac{1}{2}r + \frac{1}{6}r^3 \quad (11)$$

The HAB approach has been generalized[37] in the framework of Wertheim theory for the associating fluids. It follows that the fluid−surface correlation functions and the bulk fluid direct correlation functions are matrices of the corresponding partial correlation functions; the bulk density ρ is replaced by the density matrix whose elements represent the number densities of the particles with a given bonded state of their sites. The applications of the two-particle density formalism for dimerizing fluid and the ideal chain and ideal network approximations to the description of bulk polymerizing and network fluids, respectively, lead to a significant simplification in the theory. In particular, the Wertheim Ornstein−Zernike equation may be solved analytically in the zero-limit for the range of associative interaction 3, i.e., $x_c \to 0$, by a method analogous to that used by Baxter[49] in the case of hard-sphere model. This "sticky" limit for the association is considered with the angle-averaged associative Mayer function $\langle f_{ab}^{AS}(r)\rangle$ being the singular form:

$$\langle f_{ab}^{AS}(r)\rangle = e^{-\beta U^{HS}(r)}(\langle e^{-\beta U_{ab}^{AS}(1,2)}\rangle - 1) = K\delta(r - 1) \quad (12)$$

where K is the parameter for the strength of association between the sites. Also we have used the assumption of energetical equivalence of attractive sites $\epsilon_{ab} = \epsilon$.

Taking into account such a bulk solution for the inhomogeneous one-site dimerizing fluids,[37] we have a set of two equations for partial density profiles:

$$y_0^{DIM}(z_1, H) = 1 + 2\pi\int_{|z_1-1|}^{z_1+1}(\rho_0 S_{00}^{DIM}(|z_{12}|)h_1^{DIM}(z_2, H) + [\rho S_{00}^{DIM}(|z_{12}|) + \rho_0 S_{10}^{DIM}(|z_{12}|)]h_0^{DIM}(z_2, H))dz_2 \quad (13)$$

$$y_1^{DIM}(z_1, H) = 2\pi\int_{|z_1-1|}^{z_1+1}(\rho_0 S_{10}^{DIM}(|z_{12}|)h_1^{DIM}(z_2, H) + [\rho S_{10}^{DIM}(|z_{12}|) + \rho_0 S_{11}^{DIM}(|z_{12}|)]h_0^{DIM}(z_2, H))dz_2 \quad (14)$$

with ρ_0 being the density of undimerized particles calculated from the equation[31]

$$\rho = \rho_0 + 4\pi K^{DIM}g^{HS}(1)\rho_0^2 \quad (15)$$

where $g^{HS}(1) = (1 + {}^1/_2\eta)/(1 - \eta)^2$ is the Percus−Yevick contact value of bulk hard-sphere fluid.

The solution for bulk two-site polymerizing fluids within ideal chain approximation[39] leads to partial density profiles in the form:

$$y_0^{POL}(z_1, H) = 1 + 2\pi\int_{|z_1-1|}^{z_1+1}([2\sigma_1 S_{00}^{POL}(|z_{12}|) + \sigma_0 S_{10}^{POL}(|z_{12}|)]h_1^{POL}(z_2, H) + [\rho S_{00}^{POL}(|z_{12}|) + 2\sigma_1 S_{10}^{POL}(|z_{12}|)]h_0^{POL}(z_2, H))dz_2 \quad (16)$$

$$y_1^{POL}(z_1, H) = 2\pi\int_{|z_1-1|}^{z_1+1}([2\sigma_1 S_{10}^{POL}(|z_{12}|) + \sigma_0 S_{12}^{POL}(|z_{12}|)]h_1^{POL}(z_2, H) + [\rho S_{10}^{POL}(|z_{12}|) + \sigma_1 S_{12}^{POL}(|z_{12}|)]h_0^{POL}(z_2, H))dz_2 \quad (17)$$

where the density parameter $\sigma_0 = \sigma_1/\rho$ and σ_1 is calculated from an equation[26] similar to eq 15 by substituting σ_1 inplace of ρ_0, and K^{POL} in place of K^{DIM}.

The four-site model has been treated analytically additionally within the ideal network approximation.[28,29,36] This means that the part of the intramolecular correlations responsible for the formation of the ring-like complexes with respect to all pairs of the sites are neglected. Thus, the network may consist of crossing polymer chains with each polymer branch being described within the ideal chain approximation,[27] such as in the

case of two-site model. It is important that the obtained structure is treelike (like the Cayley tree), i.e., there is no self-crossing of the branches. Any pair of molecules in a such network is assumed to remain singly connected for any density ρ and any strength of associative interaction K. The equations for partial density profiles can be presented as[36]

$$y_0^{\mathrm{NET}}(z_1, H) = 1 + 2\pi\int_{|z_1-1|}^{z_1+1}([\sigma_T S_{00}^{00}(|z_{12}|) + 4\sigma_3 S_{10}^{00}(|z_{12}|)]h_0^{\mathrm{NET}}(z_2, H) + 4[\sigma_3 S_{00}^{00}(|z_{12}|) + 3\sigma_2 S_{10}^{00}(|z_{12}|)]h_1^{\mathrm{NET}}(z_2, H))\mathrm{d}z_2 \quad (18)$$

$$y_1^{\mathrm{NET}}(z_1, H) = 2\pi\int_{|z_1-1|}^{z_1+1}([\sigma_3 S_{00}^{00}(|z_{12}|) + 3\sigma_2 S_{10}^{00}(|z_{12}|)]h_0^{\mathrm{NET}}(z_2, H) + 4[6\sigma_2 S_{11}^{00}(|z_{12}|) + 6\sigma_2 S_{10}^{10}(|z_{12}|) + 4\sigma_3 S_{10}^{00}(|z_{12}|)]h_1^{\mathrm{NET}}(z_2, H))\mathrm{d}z_2 \quad (19)$$

where the density parameter $\sigma_2 = \sigma_3/\rho$ and σ_3 is calculated from an equation[28,29] similar to eq 15 by substituting σ_3 inplace of ρ_0 and K^{NET} in place of K^{DIM}.

The necessary functions $S_{ij}^{\mathrm{DIM}}(|z|)$, $S_{ij}^{\mathrm{POL}}(|z|)$, and $s_{ij}^{uv}(|z|)$ in eqs 13−19 are defined in the same way as in the hard-sphere case (eq 7) and are presented in the Appendix.

The functions $h_i(z, H)$ and $y_i(z, H)$ in the equations for the partial density profiles are the fluid−surface partial pair and cavity correlation functions, respectively, for the corresponding solvent model. For the case of nonbonded sites ($i = 0$), they are related in the same way as that for nonassociative hard spheres (eq 8), while, for the bonded sites ($i = 1$), the relation is

$$h_1(z, H) = \gamma(z, H)y_1(z, H) \quad (20)$$

The total density profiles or local density distributions, $\rho(z,H)$, in which we are interested, for each model are calculated as[36,37,39]

$$\rho^{\mathrm{MON}}(z, H) = \rho\gamma(z, H)Y^{\mathrm{MON}}(z, H) \quad (21)$$

$$\rho^{\mathrm{DIM}}(z, H) = \rho\gamma(z, H)[Y_0^{\mathrm{DIM}}(z, H) + \chi_0 Y_1^{\mathrm{DIM}}(z, H)] \quad (22)$$

$$\rho^{\mathrm{POL}}(z, H) = \rho\gamma(z, H)\left[Y_0^{\mathrm{POL}}(z, H) + \frac{2}{L}Y_1^{\mathrm{POL}}(z, H)\right] \quad (23)$$

$$\rho^{\mathrm{NET}}(z, H) = \rho\gamma(z, H)\left[Y_0^{\mathrm{NET}}(z, H) + \frac{4}{M}Y_1^{\mathrm{NET}}(z, H)\right] \quad (24)$$

where $\chi_0 = \rho_0/\rho$ is the fraction of undimerized particles, $L = \rho/\sigma_1$ is related to the mean number of beads in linear polymer chains (chain length), and $M = \rho/\sigma_3$ characterize the mean number of beads which form network or branched molecule.

In all the calculations that we performed and which are discussed in the next section (except the three last figures where direct comparison with experimental data are performed) we maintained the same bulk volume fraction η, occupied by different solvents that correspond to the bulk density $\rho = 0.6$, while the strength of the associative interaction K is different. For one-, two- and four-site models we choose $K^{\mathrm{DIM}} = 8$, $K^{\mathrm{POL}} = 5$, and $K^{\mathrm{NET}} = 1$. The criteria for such values of K was only to obtain an almost complete (92%) two-atomic solvent molecules for the one-site model, a sufficiently large ($L = 10$) linear chain solvent molecules for the two-site model, and a network or branched chain solvent molecules with $M = 7$ of participating monomers. For the solvent−surface interaction, we assumed $z_S = 0.5d$ and $\epsilon_S/kT = 1$ for lyophilic surfaces and $\epsilon_S/kT = 2$ in the case of lyophobic surfaces.

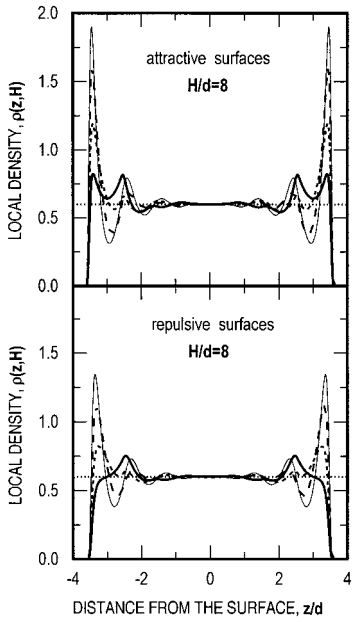

Figure 1. Density profiles of hard-sphere (thin solid line), dimer (dashed line), chain (short dashed line), and network (thick solid line) fluids between attractive and repulsive pore walls. The pore width H is eight particle diameters. The dotted lines indicate the bulk solvent density $\rho = 0.6$.

IV. Results and Discussions

Some representative results for the local density distributions of hard-sphere, dimer, chain, and network fluids in pores with attractive and repulsive fluid−surface interactions are plotted in Figure 1 as a function of distance from the surface. The surface separation that is maintained is eight monomer diameters. The local density is a convenient quantitative measure of self-arrangement of confined fluid in the molecular strata parallel to the substrate surfaces. Quite tall and narrow peaks are observed in the immediate vicinity of the substrate that reflect a well-localized first layer for spherical molecules of hard-sphere monoatomic fluid. These peaks decrease for dimers, decrease and widen for linear chains, and bifurcate and almost disappear for network fluids, especially in the case of the repulsive fluid-surface interaction. As the distance from the substrate surfaces increases, the heights of the peaks decrease and their widths increase. Nevertheless, we still can observe at least three well-defined layers even for flexible linear chains. There is a well-defined homogeneous region with the bulk density that is located in the center of the pore and covers about one particle diameter for a monatomic fluid and extends to approximately two diameters for chains and the network. This picture is nearly independent of the fluid−surface interaction. At the same time, it is worth noting that the left shoulder of the double first peak of the network fluid density profile, which we observe near the attractive surfaces, totally disappears near the repulsive surface. It means that the network film's fluid tends to separate from the substrate and becomes homogeneous faster because of the diminished influence of the confinement. Thus, we clearly observe differences in the microscopic structure of fluid films caused by complications of molecular shape and structure. What is the physical origin of these peculiarities and which consequences we can expect for experimentally accessible properties?

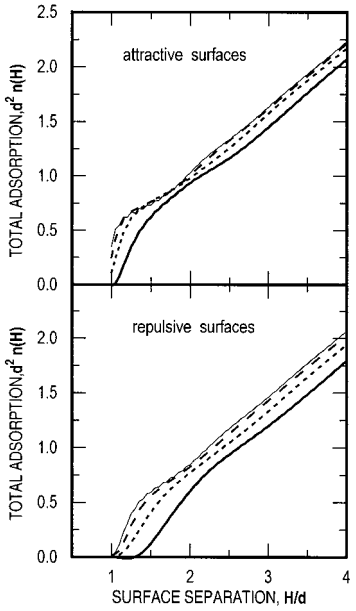

Figure 2. Total density per unit area of hard-sphere, dimer, chain, and network fluids adsorbed in a attractive and repulsive pore as a function of the surface separation. The notation of the lines is the same as that in Figure 1.

The quantity that directly influences the density distribution inside the confinement is the ability of the fluid molecules to be adsorbed into the film, i.e., the total amount of the fluid material which forms the film. The quantitative estimation of this quantity can be extracted from the integral over the density profile along the direction normal to the film surfaces:

$$n(H) = \int_0^H \rho(z, H)\mathrm{d}z \tag{25}$$

This can be called the total adsorption and is shown in Figure 2 for both types of substrate surfaces immersed in dimer, chain, and network solvents as a function of the surface separation, and is compared with the hard-sphere solvent case. At the same bulk density of the solvent, there is a higher total adsorption into the pore formed by lyophilic surfaces than that into the pore formed by lyophobic surfaces, and this adsorption is mainly due to the higher amount of the fluid entering the pore space at small separations on the order of 1−1.5 monomer diameter. The network molecules are adsorbed less into the such thin film when surfaces are attractive, and almost no adsorption is found when interaction with surfaces is repulsive. This is consistent with the behavior of the first peaks in Figure 1. When pore width is fixed, the amount of the adsorbed fluid decreases with the formation of associative complexes in the bulk solvent, i.e., from spherical monatomic molecules to dimers, chains, and networks. With an increase of the pore width, the total amount of the adsorbed fluid increases for both lyophilic and lyophobic surfaces, and adsorption curves behave very similarly.

To understand the role of associative interactions, which complicate the solvent structure as we progress from dimers to linear chains and a network molecules, we show in Figure 3a and 3b the local density distributions for films formed by such solvents at some fixed surface separations suitable for the well-defined layering in a monatomic fluid of spherical molecules. Even the small complication of the fluid structure, resulting in the change from free atoms to tangent dimers, weakens the layering because of the different orientations of the two-particle complexes even though they have a tendency to be parallel to the surface. But more drastic differences in the local structure are observed for linear chains and, especially, for network molecules and when surface separations are small. As seen, for film thickness larger than three diameters, there is a depletion of network solvent local density near the repulsive surface. Similar peculiarities have been observed recently for the mixture of hard-sphere colloids and network molecules.[50,51] Namely, hard-sphere colloidal particles immersed in a network solvent start to coagulate with increasing of network size. Moreover, simultaneously the contact value of the colloid−solvent radial distribution function goes to zero, and colloidal dispersion approach its instability related to the colloid−solvent separation.

The local density distributions of fluids of spherical molecules between two surfaces have been investigated by many authors[3−6,52,53] and are now well-understood both theoretically[54] and experimentally.[7] By means of the statistical thermodynamics description of the system, the theoretical local density distribution can be related to the observed macroscopic properties.[55] In particular, it has been shown that well-defined layering in simple fluid films with an increase of film thickness is the main reason for disjoining pressure and solvation force oscillations at small spearations. Below, we have applied the same route to obtain more insight into the changes in the behavior of macroscopic properties of the thin films due to the association.

An equilibrium property of the fluid confined by a slitlike pore that is of great interest to theories of film stability is the pressure acting on the inner side of film surfaces in the direction perpendicular to the surfaces, or local stress or normal pressure, $P_N(H)$. It can be calculated from the density profiles and as a function of film thickness, is given by[21,57,58]

$$\beta P_N(H) = -\beta \int_0^{H/2} \frac{\mathrm{d}U_S(z, H)}{\mathrm{d}z} \rho(z, H)\mathrm{d}z \tag{26}$$

The normal pressure $P_N(H)$, measured relative to the bulk pressure P_B, i.e., pressure of a homogeneous fluid that is in equilibria with film, will define the so-called disjoining pressure, $\Pi(H)$,

$$\Pi(H) = P_N(H) - P_B \tag{27}$$

The bulk pressure is one of the parameters that determine the thermodynamic state of the bulk fluid. It can be calculated independently or can be identified as a limiting value of normal pressure acting between surfaces at infinite separation. To satisfy the self-consistency of the numerical procedure we used the second possibility i.e., we assume $P_B \equiv P_N(H \to \infty)$. Particularly, to calculate bulk pressure we used the surface separations of 10 solvent particle diameters, which according to Figure 1 provides us with well-defined homogeneous region.

In Figure 4 we present our calculations of the disjoining pressure vs film thickness for all four solvent films confined by attractive and repulsive surfaces. The disjoining pressure oscillates between positive and negative values and causes the adsorbed fluid to climb or spread on surfaces. The dependence of the amplitude, periodicity, and decay of oscillations on the conformation of the solvent molecules and type (lyophilic/lyophobic) of confinement is evident. It will influence the stability of the film, since the zeros of the disjoining pressure (thickness at which the force exerted by the film on the surfaces equals the bulk pressure on the outer side of the surfaces) are related to the stable or nonstable thickness of the film.

To understand the qualitative trends in the film stability initiated by the geometry of solvent molecules, we applied the Derjaguin approximation.[56] According to Derjaguin,[56] the dis-

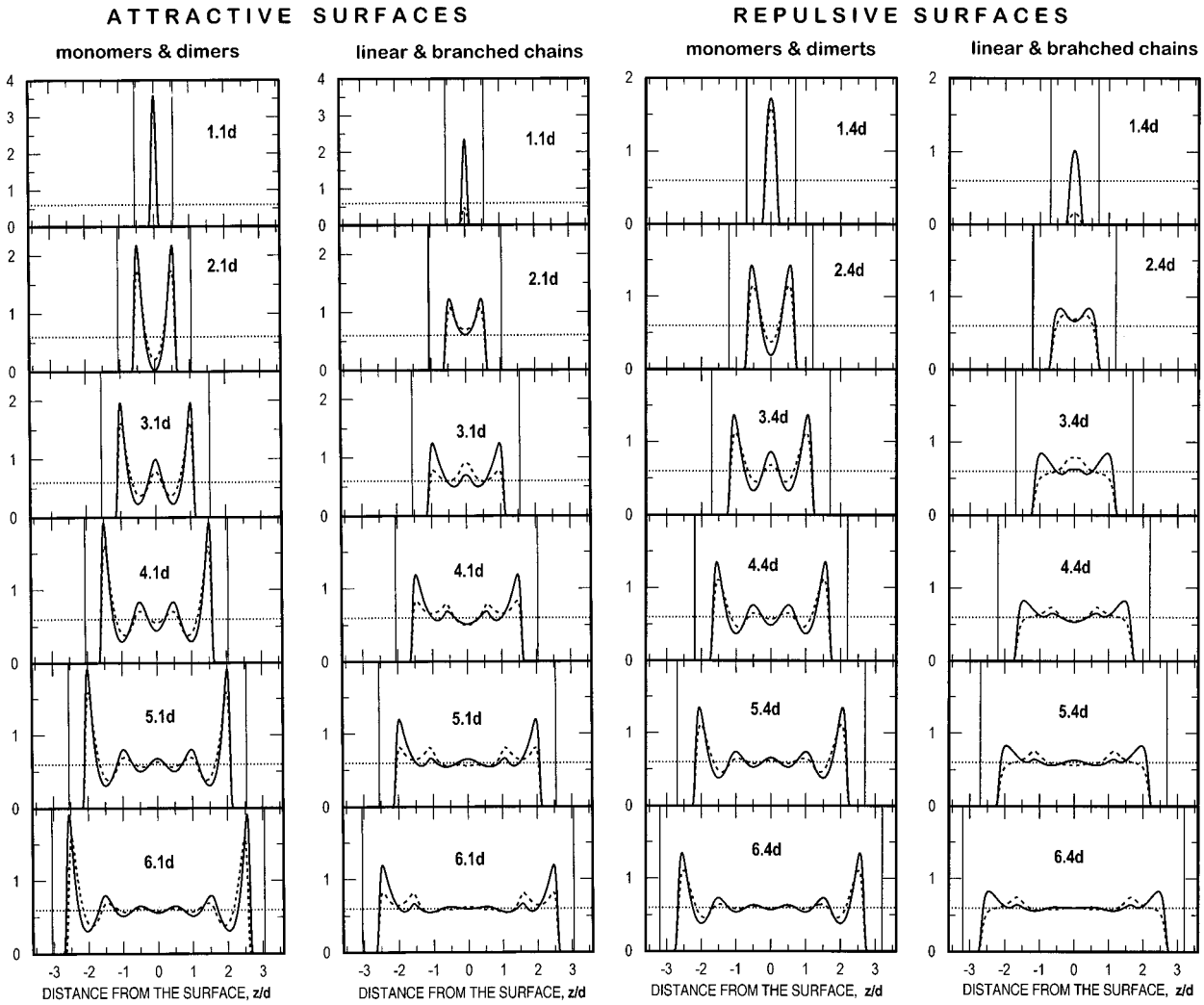

Figure 3. (a) Local density distribution of hard-sphere and dimer fluid films (left part) and linear chain and network fluid films (right part) confined by attractive surfaces at different values of the surface separation. The surface separation H, in units of hard-sphere diameters, is written in the fragments. The vertical thin solid lines on each fragment indicate the position of confined surfaces, while the dotted lines correspond to the bulk solvent density $\rho = 0.6$. (b) Local density distribution of hard-sphere and dimer fluid films (left part) and linear chain and network fluid films (right part) confined by repulsive surfaces at different values of the surface separation. The surface separation H in units of hard-sphere diameters, is written in the fragments. The vertical thin solid lines on each fragment indicate the position of confined surfaces, while the dotted lines correspond to the bulk solvent density $\rho = 0.6$.

joining pressure can be measured by displacing one of the surfaces a distance ΔH and the work per unit area to bring the surfaces from infinity to the separation H, or the thermodynamic energy change of the system (excess film free energy) $F(H)$ can be calculated as

$$\frac{F(H)}{R} = 2\pi \int_H^\infty \Pi(H')\mathrm{d}H' \qquad (28)$$

where R is the curvature of macroscopic surface. The quantity $F(H)/R$ can be determined directly in "surface force apparatus" and is called the solvation force.

Since all complexes formed in our associative solvents are tangent, any effects of the excluded volume due to penetration are not presented. The extraction of the hard-sphere contribution from the $F(H)$ will give information about the association-induced contribution to the force. These results are presented in Figure 5 and compared with the hard-sphere solvent force. The association induced contribution is of the same order as the hard-sphere result and is the smallest for the dimer solvent and grows, going from linear to branched chains. This association produced an oscillating force that has the opposite sign of the hard-sphere contribution and will result in a decrease in the magnitude, shift in the phase, and increase in the periodicity of the oscillations of the total force exerted by dimer, linear chain, and network films which are shown in Figure 6. The energy law is similar in hard-sphere (see Figure 5) and dimer solvents, but changes are reflected in the flexible chains and network solvents. In general, for all types of solvents, the solvation force is a damped oscillatory function of the thickness of film but with a different periodicity. The spherical monomers and short dimers are able to pack efficiently and, because of this fill in the space between the surfaces, down to very thickened films; the observed range of oscillations is up to four particle diameters and the periodicity is approximately equal to the particle diameter, i.e., unity. The oscillations in the flexible chain solvent are weaker and periodicity grows to about of two bead diameters. The solvation force of network solvent at small surface spearations (on the order of 1.5 bead diameter) is shifted more to the repulsive region in the case of lyophilic film surfaces and is attractive for the same film thickness when the fluid−surface interaction is repulsive. When the surface separation

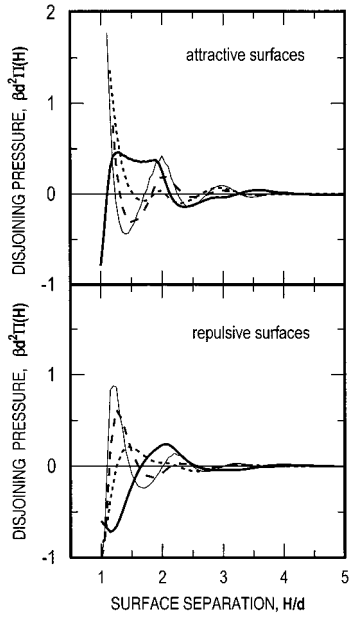

Figure 4. Disjoining pressure exerted by a hard-sphere, dimer, linear chain and network films, confined between flat parallel attractive (part a) and repulsive (part b) surfaces as a function of the surface separation. The notation of the lines is the same as that in Figure 1.

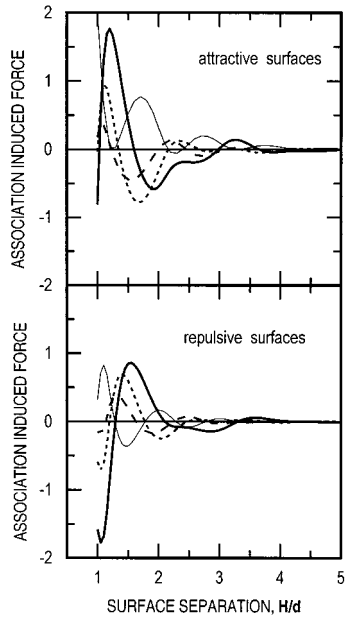

Figure 5. Association induced solvation forces between attractive (part a) and repulsive (part b) surfaces immersed in dimer, linear chain, and network fluids as a function of the surface separation. The thin solid line shows the hard core exclusion force between the same surfaces in hard-sphere solvent, calculated using the Derjaguin approximation. The notation of the remaining lines is the same as that in Figure 1.

increases, the films formed by chain and network solvents stimulate attraction for both kind of surfaces, though for the lyophilic surfaces this effect is more pronounced. It is important to mention that these results confirm the conclusions derived previously in experiments[7] as well as in computer simulations.[14−17]

In Figures 7 and 8 we show some results that can be directly related to experimental data.[7] To obtain these results we have added to the force (eq 28) the van der Waals contribution (the so-called Hamaker force) arising from the direct interaction between the surfaces.[7] Thus, the calculated force, which can be compared with the observed data, has the form

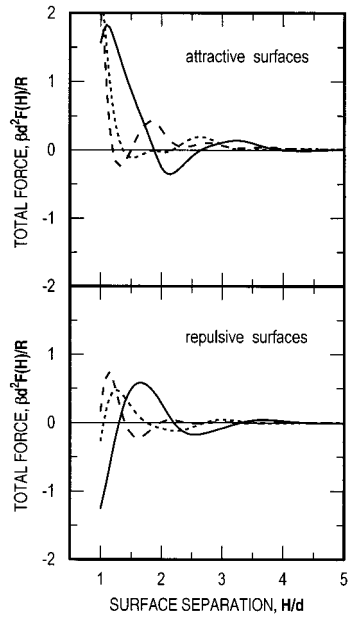

Figure 6. Total solvation force between attractive (part a) and repulsive (part b) surfaces immersed in dimer, linear chain and network solvents calculated using the Derjaguin approximation, as a function of the surface separation. The notation of the lines is the same as that in Figure 1.

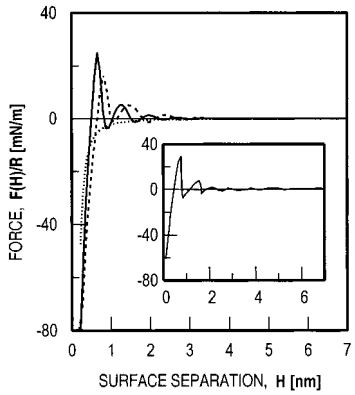

Figure 7. Force (including the van der Waals term) between two macroscopic surfaces in a fluid of hard spheres of diameter $d_{HS} = 0.9$ nm (dashed line) and in a dimer fluid of diameter $d_{DIM} = 0.72$ nm (solid line). The dotted line shows the van der Waals contribution. The density in both cases is $\bar{\rho}d_{HS}^3 = \bar{\rho}d_{DIM}^3 = 0.7$. The diameter of the dimer atoms has been chosen from the condition that volume of the hard-sphere molecule is the same as the volume of dimer molecule, i.e., $d_{HS}^3 = d_{DIM}^3 + 1.5d_{DIM}^2L^2 - 0.5d_{DIM}^3L^3$. The both results can be compared (inset) with the measured force between two cylindrically curved mica surfaces in octamethylcyclotetrasiloxane (OMCTS) with molecular diameter $d \approx 0.9$ nm. The inset is adapted from Figure 5 of ref 52.

$$\frac{F(H)}{R} = -\frac{A}{6H^2} + 2\pi\int_H^\infty \Pi(H')\mathrm{d}H' \qquad (29)$$

where A is Hamaker constant. In the theoretical model the film is confined in the z-direction between two substrates with flat surfaces. In the "surface force apparatus" the measurements are performed between the surfaces of two crossed cylinders. However, by using Derjaguin approximation,[56] the crossed-cylinder configuration can be mapped very precisely (it is exact in the limit of macroscopic spheres,[59] i.e., when $R \to \infty$) onto two flat surfaces confinement. In experiment the surface of each macroscopic confinement can be covered by a thin mica sheet

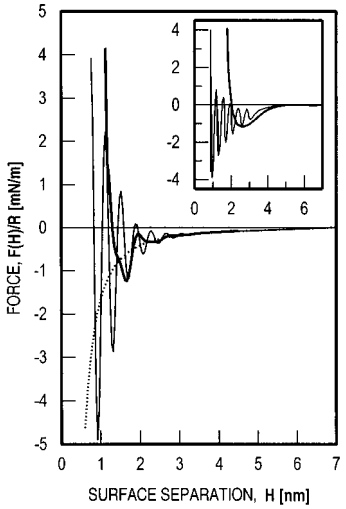

Figure 8. Force (including the van der Waals term) between two attractive macroscopic surfaces in a linear chain fluid ($\bar{\rho}d^3 = 0.85$, $d = 0.4$ nm, $K = 5$), thin solid line, and in a network fluid ($\bar{\rho}d^3 = 0.8$, $d = 0.45$ nm, $K = 1$), thick solid line. The dotted line shows the van der Waals contribution. The results can be compared (inset) with the measured force laws between mica surfaces in straight-chained liquid alkanes such as *n*-tetradecane and *n*-hexadecane (molecular width $d \approx 0.4$ nm) and in the branched alkane (iso-paraffin) 2-methyloctadecane. The inset is adapted from Figure 13.5 of ref 7, page 272.

and coated with a monolayer of condensed substance to regulate the strength of interaction with solvents.

In Figure 7 we plot the calculated forces between two surfaces immersed in hard-sphere and dimer solvents. Taking a hard-sphere diameter $d_{HS} = 0.9$ nm roughly simulates octamethylcyclotetrasiloxane (OMCTS) which is the most investigated system by experimental methods.[7,52,53] OMCTS is an inert silicone liquid whose nonpolar molecules are quasi-spherical, and a hard-sphere or Lennard-Jones fluid films serve as a very suitable model. Using the integral equation technique, the case of hard-sphere solvent and its relation to Horn and Israelachvili[52] experiment has been reported already by Henderson and Lozada-Cassou[1] for OMCTS, and has been discussed by Israelachvili.[7] It has been pointed out that the calculated force laws are quite similar to the experimental results. To study the effect of the shape, we assumed that OMCTS molecule is elongated in some direction and that can be represented by a dimer. Choosing the diameter of the dimer atoms d_{DIM} on the condition that the volume of the dimer molecule is the same as that of the hard-sphere molecule, i.e.,

$$d_{HS}^3 = \frac{3}{2}d_{DIM}^2 + \frac{1}{2}d_{DIM}^3 \qquad (30)$$

we performed a calculation of the solvation force in a dimer solvent with $d_{DIM} = 0.73$ nm and hard-sphere solvent with $d_{HS} = 0.9$ nm, maintaining the same particle bulk number density $\bar{\rho}d_{HS}^3 = \bar{\rho}d_{DIM}^3 = 0.7$ in both cases. The solvent−surface interaction was attractive according to eq 5 with $\alpha = 1$, $\epsilon_S/kT = 1$, and $z_S = 0.5d_{HS}$ or $0.5d_{DIM}$. In a some sense, such a set of hard-sphere and dimer atom diameters corresponds to taking into account the effect of the non-sphericity of the OMCTS molecules. The agreement of the calculated and experimental results is improved (for comparison see inset in Figure 7).

Figure 8 shows the calculated results for the force between two macroscopic surfaces in chain and network solvents. These two results can be compared with measured force laws between mica surfaces observed by Christenson et al.[60] across straight-chained liquid alkanes such as *n*-tetradecane and *n*-hexadecane

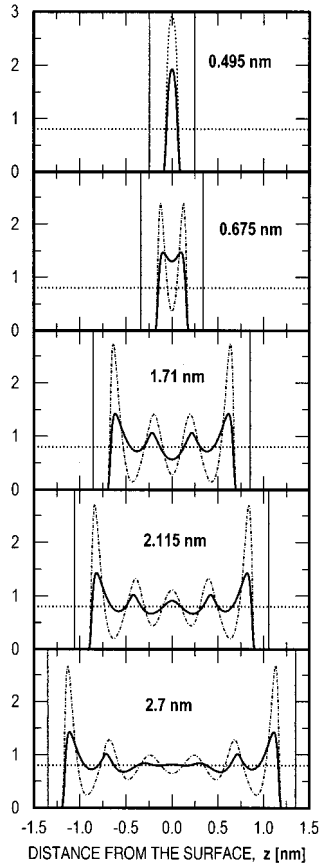

Figure 9. Density distribution in network (solid line) and hard-sphere (short dashed line) films correspond to the force law shown in Figure 8. The surface separation H in nanometers is written in the fragments. The vertical thin solid lines on each fragment indicate the position of confined surfaces, while the dotted lines correspond to the bulk solvent density $\rho = 0.8$.

(molecular width $d \approx 0.4$ nm) and by Gee and Israelachvili[9] across the branched alkane (iso-parafin) 2-methyloctadecane. To approximate experimental results with our model, we chose the parameters $\bar{\rho}d^3 = 0.85$, $K = 5$, $\epsilon_S/kT = 0.05$, $z_S = 0.7d$, $d = 0.4$ nm for linear chain solvent, and $\bar{\rho}d^3 = 0.8$, $K = 1$, $\epsilon_S/kT = 0.01$, $z_S = 0.7d$, $d = 0.45$ nm to model branched chains. We see that the force law in linear chain fluid still exhibits oscillatory behavior, similar to the film of spherical molecules, but is shifted to the attraction region. The force mediated by network fluid is completely different: it is repulsive until a thickness of about 1 nm (on the order of two-three single bead diameters) and than becomes always attractive and almost totally monotonic. The qualitative agreement between the calculated and experimental results is quite good (for the comparison see inset in Figure 8).

To understand why the network solvent eliminates force oscillations, we show in Figure 9 the local density distributions for the force law discussed in Figure 8. The repulsive force between lyophilic surfaces at small separations originates from the first adsorbed layer of solvent molecules and extends on the separations of order of the thickness of this layer. For separations intermediate between first and second layers, the film undergoes a local reorganization, and the attractive interaction between confining surfaces dominates. The existence of layer ordering near substrate can be identified from the oscillations of local density *relatively to the bulk density*, that is the case of the film formed by spherical monomers, dimers, or even linear chains (see Figure 3). Two density maxima that we observe in a network film at small thickness can be treated

as the splitting of a rather thick first layer only, which remains disordered or amorphous. The local density in such film are always higher than the corresponding bulk density, and the force exerted by the film on the surfaces is repulsive. For the results discussed in Figure 8 such a disordered first layer of network film is extended until around 1.5 nm. At this thickness the local density distribution starts exhibit relatively deep failure (Figure 9), that causes attraction between constraining boundaries. At larger thickness, the density distribution behaves as usual.

The fact that the chain structure of the solvent molecule in which the surfaces are immersed can result in an attractive or repulsive contribution to the solvation force has been pointed out by Israelachvili[7] who calls this effect a positive or a negative solvation force. The existence of prevailing attraction force in linear chain solvent has been supported also by recent computer simulation results by Dijkstra.[14] However, to our knowledge, this is the first theoretical treatment of these effects.

Acknowledgment. Y.D. and A.T. acknowledge support of DGAPA of the UNAM, Grant IN 111597. This work also has been supported in part by the National Science Foundation, Grants CHE 96-01971 and CHE 98-13729, and the donors of the Petroleum Research Found, administrated by the American Chemical Society, Grant ACS-PRF 31573-AC9. The numerical calculations have been performed by using computer facilities of DGSCA of the UNAM and the BYU computational chemistry parallel computer.

Appendix

***S*-Functions of Associating Fluids.** We present here the analytical expressions for *S*-functions of model associating fluids we used to calculate the local density distributions. These functions have been extracted from the solutions of homogeneous problem for these models.

(*a*) *One-Site Dimerizing Model.*

$$S_{00}^{\mathrm{DIM}}(r) = S^{\mathrm{MON}}(r) + 2\pi\rho_0\left(\frac{1}{2}A_1a_0a_1 + \frac{1}{2}(A_2 + A_3)(a_0b_1 + a_1b_0) + 2A_4b_0b_1\right) \quad \text{(A1)}$$

$$S_{10}^{\mathrm{DIM}}(r) = \frac{1}{2}a_1(r^2 - 1) + b_1(r - 1) - 2\pi\rho_0K^{\mathrm{DIM}}g^{\mathrm{HS}}(1)(A_5a_0 + 2A_6b_0) \quad \text{(A2)}$$

$$S_{11}^{\mathrm{DIM}}(r) = K^{\mathrm{DIM}}g^{\mathrm{HS}}(1) \quad \text{(A3)}$$

(b) Two-Site Polymerizing Model.

$$S_{00}^{\mathrm{POL}}(r) = S^{\mathrm{MON}}(r) + 8\pi\sigma_1\left(\frac{1}{2}A_1a_0a_1 + \frac{1}{2}(A_2 + A_3)(a_0b_1 + a_1b_0) + 2A_4b_0b_1\right) + 4\pi\sigma_0\left(\frac{1}{4}A_1a_1^2 + \frac{1}{2}a_1b_1(A_2 + A_3) + A_4b_1^2\right) \quad \text{(A4)}$$

$$S_{10}^{\mathrm{POL}}(r) = \frac{1}{2}a_1(r_2 - 1) + b_1(r - 1) - 2\pi\sigma_1K^{\mathrm{POL}}g^{\mathrm{HS}}(1)\left(\frac{1}{2}A_5a_0 + A_6b_0\right) - 2\pi\sigma_0K^{\mathrm{POL}}g^{\mathrm{HS}}(1)\left(\frac{1}{2}A_5a_1 + A_6b_1\right) \quad \text{(A5)}$$

$$S_{12}^{\mathrm{POL}}(r) = K^{\mathrm{POL}}g^{\mathrm{HS}}(1) - 2\pi\sigma_0(K^{\mathrm{POL}}g^{\mathrm{HS}}(1))^2(1 - r) \quad \text{(A6)}$$

(c) Four-Site Network-Forming Model.

$$S_{00}^{00}(r) = S^{\mathrm{MON}}(r) + 8\pi\sigma_3\left(\frac{1}{2}A_1a_0a_1 + \frac{1}{2}(A_2 + A_3)(a_0b_1 + a_1b_0) + 2A_4b_0b_1\right) + 24\pi\sigma_2\left(\frac{1}{4}A_1a_1^2 + \frac{1}{2}a_1b_1(A_2 + A_3) + A_4b_1^2\right) \quad \text{(A7)}$$

$$S_{10}^{00}(r) = \frac{1}{2}a_1(r^2 - 1) + b_1(r - 1) - 2\pi\sigma_3K^{\mathrm{NET}}g^{\mathrm{HS}}(1)\left(\frac{1}{2}A_5a_0 + 2A_6b_0\right) - 2\pi\sigma_2K^{\mathrm{NET}}g^{\mathrm{HS}}(1)(3A_5a_1 + 6A_6b_1) \quad \text{(A8)}$$

$$S_{11}^{00}(r) = -4\pi\sigma_2(K^{\mathrm{NET}}g^{\mathrm{HS}}(1))^2(1 - r) \quad \text{(A9)}$$

$$S_{01}^{10}(r) = K^{\mathrm{NET}}g^{\mathrm{HS}}(1) - 8\pi\sigma_2(K^{\mathrm{NET}}g^{\mathrm{HS}}(1))^2(1 - r) \quad \text{(A10)}$$

The coefficients a_0, b_0 and A_1, A_2, A_3, A_4 are the same as for hard spheres (eq 11), and

$$A_5 = -\frac{2}{3} + r - \frac{1}{3}r^3, \quad A_6 = -\frac{1}{2} + r - \frac{1}{2}r^2 \quad \text{(A11)}$$

The coefficients a_1 and b_1 in the case of one-site model are calculated as

$$a_1 = -\rho_0K^{\mathrm{DIM}}\frac{2\pi g^{\mathrm{HS}}(1)}{1 - \eta}, \quad b_1 = \rho_0K^{\mathrm{DIM}}\frac{\pi g^{\mathrm{HS}}(1)}{1 - \eta} \quad \text{(A12)}$$

while for two- and four-site model prefactor ρ_0K^{DIM} has to be substituted by σ_1K^{POL} and σ_3K^{NET}, respectively.

References and Notes

(1) Henderson, D.; Lozada-Cassou, M. *J. Colloid Interface Sci.* **1986**, *114*, 180.
(2) Henderson, D. *J. Colloid Interface Sci.* **1988**, *121*, 486.
(3) Magda, J. J.; Tirrell, M.; Davis, H. T. *J. Chem. Phys.* **1985**, *83*, 1888.
(4) Luzar, A.; Bratko, D.; Blum, L. *J. Chem. Phys.* **1987**, *86*, 2955.
(5) Wertheim, M., Blum, L., and Bratko, D. In *Micellar Solutions and Microemulsions*; Chen, S.-H., Rajagopalan, R., Eds.; Springer: New York, 1990; Chapter 6.
(6) Bordarier, P.; Rousseau, B.; Fuchs, A. N. *J. Chem. Phys.* **1997**, *106*, 7295.
(7) Israelachvili, J. N. *Intermolecular and Surface Forces*, 2nd ed.; Academic Press: London, 1992.
(8) Israelachvili, J. N.; McGuiggan *Science* **1988**, *241*, 795.
(9) Gee, M. L.; Israelachvili, J. N. *J. Chem. Soc., Faraday Trans.* **1990**, *86*, 4049.
(10) Granick, S. *Science* **1991**, *253*, 1374.
(11) Christenson, H. K. *Chem. Phys. Lett.* **1985**, *118*, 455.
(12) Israelachvili, J. N.; Kott, S. J. *J. Chem. Phys.* **1988**, *88*, 7162.
(13) Wang, Y.; Hill, K.; Harris, J. G. *J. Chem. Phys.* **1994**, *100*, 3276.
(14) Dijkstra, M. *J. Chem. Phys.* **1997**, *107*, 3277.
(15) Gao, J.; Luedtke; Landman, U. *J. Phys. Chem.* **1997**, *101*, 4013.
(16) Gao, J.; Luedtke; Landman, U. *J. Phys. Chem.* **1997**, *106*, 4309.
(17) Dickman, R.; Yethiraj, A. *J. Chem. Phys.* **1994**, *100*, 4683.
(18) Kjellander, R.; Sarman, S. *Mol. Phys.* **1990**, *70*, 215.
(19) Kjellander, R.; Sarman, S. *Mol. Phys.* **1991**, *74*, 665.
(20) Sarman, S. *J. Chem. Phys.* **1990**, *92*, 4447.
(21) Walley, K. P.; Schweizer, K. S.; Peanasky, J.; Granick, S. *J. Chem. Phys.* **1994**, *100*, 3361.
(22) Trokhymchuk, A.; Pizio, O.; Sokolowski, S.; Henderson, D. *Mol. Phys.* **1995**, *86*, 53.
(23) Trokhymchuk, A.; Pizio, O.; Sokolowski, S. *J. Colloid Interface Sci.* **1996**, *178*, 436.
(24) Kierlik, E.; Rosinberg, M. L. *J. Chem. Phys.* **1994**, *100*, 1716.
(25) Phan, S.; Kierlik, E.; Rosinberg, M. L.; Yethiraj, A.; Dickman, R. *J. Chem. Phys.* **1995**, *102*, 2141.
(26) Wertheim, M. S. *J. Chem. Phys.* **1989**, *82*, 2929.
(27) Chang, J.; Sandler, S. *J. Chem. Phys.* **1995**, *102*, 437; **1995**, *103*, 3196.

(28) Vakarin, E.; Duda, Y.; Holovko, M. F. *Mol. Phys.* **1997**, *90*, 611.
(29) Duda, Y.; Segura, C. J.; Vakarin, E.; Holovko, M. F.; Chapman, W. *J. Chem. Phys.* **1998**, *108*, 9168.
(30) Cummings, P.; Stell, G. *Mol. Phys.* **1984**, *51*, 253.
(31) Wertheim, M. S. *J. Stat. Phys.* **1986**, *42*, 459, 477.
(32) Kalyuzhnyi, Y.; Stell, G. *Mol. Phys.* **1993**, *78*, 1247.
(33) Kolafa, J.; Nezbeda, I. *Mol. Phys.* **1987**, *61*, 161.
(34) Nezbeda, I.; Kolafa, J.; Kalyuzhnyi, Y. V. *Mol. Phys.* **1989**, *68*, 143.
(35) Ghonasgi, D.; Chapman, W. G. *Mol. Phys.* **1993**, *79*, 291.
(36) Vakarin, E.; Holovko, M. F.; Duda, Y. *Mol. Phys.* **1997**, *97*, 203.
(37) Holovko, M. F.; Vakarin, E. *Mol. Phys.* **1995**, *84*, 1057.
(38) Vakarin, E.; Duda, Y.; Holovko, M. F. *J. Chem. Phys.* **1997**, *107*, 5569.
(39) Segura, C.; Vakarin, E.; Chapman, W.; Holovko, M. *J. Chem. Phys.* **1998**, *108*, 4837.
(40) Pizio, O.; Henderson, D.; Sokolowski, S. *J. Phys. Chem.* **1995**, *99*.
(41) Kovalenko, A.; Trokhymchuk, A.; Pizio, O.; Henderson, D. *Mol. Phys.* **1996**, *89*, 1765.
(42) Henderson, D.; Abraham, F. F.; Barker, J. A. *Mol. Phys.* **1976**, *31*, 1291.
(43) Zhou, Y.; Stell, G. *Mol. Phys.* **1989**, *66*, 767.
(44) Schoen, M.; Diestler, D. J.; Cushman, J. H. *J. Chem. Phys.* **1994**, *101*, 6865.
(45) Chmiel, G.; Karykowski, K.; Patrykiejew, A.; Rzysko, W.; Sokolowski, S. *J. Chem. Soc., Faraday Trans. II* **1994**, *90*, 1153.
(46) Sokolowski, S.; Fisher, J. *J. Chem. Soc., Faraday Trans. II* **1993**, *89*, 789.
(47) Pospisil, R.; Sys, J.; Malijevsky, A.; Labik, S. *Mol. Phys.* **1992**, *75*, 26.
(48) Christenson, H. K. *J. Chem. Phys.* **1983**, *78*, 6906.
(49) Baxter, R. J. *J. Chem. Phys.* **1968**, *49*, 2770.
(50) Duda, Y. *J. Colloid Interface Sci.* **1998**, *208*, 279.
(51) Duda, Y. *J. Colloid Interface Sci.* **1999**, *213*, 498.
(52) Horn, R. G.; Israelachvili, J. N. *J. Chem. Phys.* **1981**, *75*, 1400.
(53) Gee, M. L.; McGuiggan, P. M.; Israelachvili, J. N.; Honda, A. M. *J. Chem. Phys.* **1990**, *93*, 1895.
(54) Schoen, M.; Gruhn, T.; Diestler, D. J. *J. Chem. Phys.* **1998**, *109*, 301.
(55) The theoretically calculated local density can be related to the normal pressure $P_N(z)$ or normal stress, i.e., the force applied to unit area of the surfaces. The relationship between $P_N(z)$ and the measured solvation force is not immediately obvious, although it was derived by Derjaguin.[56] For more discussion of this, for example, see ref 54.
(56) Derjaguin, B. V. *Kolloid Zh.* **1934**, *69*, 155.
(57) Henderson, D.; Blum, L.; Lebowitz, J. L. *J. Electroanal. Chem.* **1979**, *102*, 315.
(58) Rickayzen, G. *Mol. Phys.* **1985**, *55*, 161.
(59) Gotzelmann, B.; Evans, R.; Dietrich, S. *Phys. Rev. E* **1998**, *57*, 6785.
(60) Christenson, H. K.; Gruen, D. W. R.; Horn, R. G.; Israelachvili, J. N. *J. Chem. Phys.* **1987**, *87*, 1834.